Available online at www.sciencedirect.com
SCIENCE DIRECT®
Journal of Computational Physics 203 (2005) 467–492
JOURNAL OF COMPUTATIONAL PHYSICS
www.elsevier.com/locate/jcp

Unidirectional transparent signal injection in finite-difference time-domain electromagnetic codes –application to reflectometry simulations

F. da Silva [a,*], S. Heuraux [b], S. Hacquin [a,1], M.E. Manso [a]

[a] *Associação EURATOM/IST—Centro de Fusão Nuclear, Instituto Superior Técnico, 1046-001 Lisboa, Portugal*
[b] *Laboratoire de Physique des Milieux Ionisés et Applications Unité du CNRS 7040, Université Henri Poincaré, Nancy 1, BP 239, 54506 Vandœuvre Cedex, France*

Received 2 July 2004; received in revised form 7 September 2004; accepted 7 September 2004
Available online 2 November 2004

Abstract

We present a novel numerical signal injection technique allowing unidirectional injection of a wave in a wave-guiding structure, applicable to 2D finite-difference time-domain electromagnetic codes, both Maxwell and wave-equation. It is particularly suited to continuous wave radar-like simulations. The scheme gives an unidirectional injection of a signal while being transparent to waves propagating in the opposite direction (directional coupling). The reflected or backscattered waves (returned) are separated from the probing waves allowing direct access to the information on amplitude and phase of the returned wave. It also facilitates the signal processing used to extract the phase derivative (or group delay) when simulating radar systems. Although general, the technique is particularly suited to swept frequency sources (frequency modulated) in the context of reflectometry, a fusion plasma diagnostic. The UTS applications presented here are restricted to fusion plasma reflectometry simulations for different physical situations. This method can, nevertheless, also be used in other dispersive media such as dielectrics, being useful, for example, in the simulation of plasma filled waveguides or directional couplers.

1. Introduction

Frequency modulated (FM) reflectometry is a technique widely used in fusion plasmas to measure the electron density profile [1] and to extract information on density fluctuations [2]. Simulations are essential

* Corresponding author. Tel.: +351218419080; fax: +351218417819.
E-mail address: tanatos@cfn.ist.utl.pt (F. da Silva).
[1] Work address: JET-EFDA, Culham Science Center, Abingdon DX14 3DB, UK.

0021-9991/$ - see front matter © 2004 Elsevier Inc. All rights reserved.
doi:10.1016/j.jcp.2004.09.002

to understand and correctly interpret the measured signals. To achieve this, it is necessary to have a well adapted signal injection, in our application of 2D finite-difference time-domain codes: (i) based on the Yee's algorithm (Maxwell code) [3]; (ii) and a wave equation code. It is especially important that a continuous injected wave comes back unaltered to the emitting structure, also used as a receiver, since it contains the information on the density plasma with a high dynamic computational range as possible and should not be modified by numerical artefacts due to signal injection. The signal injection has to satisfy the following conditions at any time: (i) the injected wave has to be unidirectional; (ii) the input signal can be modulated in frequency and/or amplitude or can also have a fixed frequency; (iii) and the back wave should go through the signal injection position without perturbation. The source will be embedded on an emitting structure (an antenna horn for instance) to provide directionality to the emitted wave. This kind of signal injection will be called *unidirectional transparent source* (UTS) in the following. To implement it, we will resort to the concept of impulsive response of a system. A similar approach has been proposed in [4] in order to implement a transparent source for waveguide propagation structures. In our work, we deal with an open structure (antenna) and we introduce the concept of unidirectionality of the source. Our line source (screen) will excite the selected input function unidirectionally in the waveguide. The implementation of such a scheme (waveguide and UTS) is an effective way of simulating a directional coupler. The use of this microwave device is necessary to simulate the monostatic reflectometers (one antenna for emission and reception) [5]. The use of an UTS is of utmost importance in the simulation of reflectometry in fusion plasmas, particularly continuous wave frequency modulated (CWFM) reflectometry for density plasma evaluation.

The accurate knowledge of the reflected signal in plasma reflectometry is very important when trying to understand the amplitude perturbations suffered by the wave in perturbed media or the amplitude dropouts of the wave due to interference phenomena for instance. These effects are completely lost if we have the simultaneous presence of the reflected and emitted signals, the latter with much higher amplitude completely masking the amplitude signatures present in the returned signal (low dynamic computational range). The measurements of the phase difference between the emitted and returned signals although possible, are more complicated with the presence of both signals. The UTS permits to reach the phase and amplitude at each time step in the case of frequency sweep if the back-end of the antenna is associated to a transparent boundary condition, preventing the wave from being reflected and re-injected into the grid [6,7]. Having access to the isolated return signal also permits to simulate the different detection methods used in reflectometry: homodyne or heterodyne setups, phase and quadrature detection, level detection (pulse reflectometry), essential to simulate the different reflectometry experiments (not just the propagation part). In fact, the accessible signals are these post-detection lower frequency signals to which different signal processing techniques are applied in order to extract the relevant information about the plasma (e.g., density profile and density fluctuations).

The use of an UTS is not always necessary as shown in literature. In the main reflectometry simulations, we can distinguish different kinds of signal injection, the simplest one being the hard point corresponding to a single point emitting omni-directionally (within the grid discretization). The hard point has been used to solve the one-dimensional Helmholtz [8] and sophisticated tools are needed to extract the phase and amplitude of the backscattered wave. One can find it also in the first 2D FDTD reflectometry simulation [9] where it is assumed that the source does not perturb the field computation. That can be justified only for small computation time as long as the back wave does not return to the source. To avoid this trouble, the simplest way is using an absorbing boundary conditions corresponding to spatial electric field distribution as input, this has been used to describe the cross-polarization scattering [10] but it can be applied only for a short pulse. The directionality of the input wave has been obtained in the 1D wave equation for ultra-short pulse reflectometry [11] and also in 2D ultra-short pulse reflectometry [12,13] giving the electric field for two sequential time steps over all vacuum space. This method can be used only on short time input. In 2D problems, a hard line has been used to define an emitting mode in a waveguide (often the mode TE_{10}) in 2D Helmholtz solver [14,15] or 2D FDTD [16,17] with a perfect match layer PML [7]. In the case of 2D

transient matching layer (TML) [18], the equivalent 2D field distribution in phase and amplitude is given over the antenna aperture just on the edge of a perfect match circuit. Recent works [19–21] used Huygens surface [22,23] to launch a unidirectional Gaussian beam, to separate the back wave and the incident wave and to introduce sub-domains. This last method computes at each time step the source terms on the Huygens surface [20]. In the case of an emitting structure, the closed Huygens surface cannot be easily implemented in an antenna and requires multi-domains (regions). All these problems lead us to the implementation of a unidirectional injection of the wave in the waveguide to have the widest computational dynamic range possible with the smallest increase on computational time. The grid points placed on the back of the injection line do not receive the emitted signal. An important point is that this emission line source must be transparent to the backward (reflected) signal which propagates in the opposite direction allowing the recuperation in the waveguide of the returned signal, isolated from the emitting signal. This signal injection technique takes very little computing time compared to the total computing time.

This paper is organized as follows: In Section 2, we describe the FDTD algorithm for two solvers (Maxwell and wave-equation) to recall the basis used in the UTS and principles of the UTS in Section 3. The implementation of the UTS and its use on an open open radiating structure are presented in Sections 4 and 5. Section 6 is devoted to three examples illustrating the use of the UTS. We conclude this paper by a discussion of the limitations, the possibilities offered by UTS in the fusion plasma reflectometry simulations and the possible extension of this method.

2. Numerical schemes for wave propagation in vacuum

The initial conditions for unidirectional signal emission proposed in this paper have been implemented and tested with two different codes solving the Maxwell equations. The numerical schemes of these codes are recalled in this section in order to facilitate the understanding of the UTS scheme.

2.1. Maxwell scheme FDTD code solving the Maxwell equations

Considering the Maxwell curl equations in a vacuum written in MKS units

$$\nabla \times \mathbf{E} = -\frac{\partial \mathbf{B}}{\partial t}, \tag{1}$$

$$\nabla \times \mathbf{B} = \varepsilon_0 \mu_0 \frac{\partial \mathbf{E}}{\partial t}. \tag{2}$$

Assuming propagation in the xy-plane and electromagnetic fields constant along the z-axis we have, for the transverse magnetic (TM) propagation mode (E_z, B_x, B_y), the following set of equations:

$$\begin{aligned} \frac{\partial B_x}{\partial t} &= -\frac{\partial E_z}{\partial y}, \\ \frac{\partial B_y}{\partial t} &= \frac{\partial E_z}{\partial x}, \\ \frac{\partial E_z}{\partial t} &= \frac{1}{\varepsilon_0 \mu_0}\left(\frac{\partial B_y}{\partial x} - \frac{\partial B_x}{\partial y}\right). \end{aligned} \tag{3}$$

Let $F(x,y,t)$ be the field quantity F at position (x,y) at time t. The various fields are sampled at discrete positions $(i\Delta x, j\Delta y)$ and instants $t = n\Delta t$. In the rest of this paper, we will denote $F(i\Delta x, j\Delta y, n\Delta t)$ by $F^n(i,j)$ and refer to its location (i,j) at the nth time step. The scheme presented is the *classical* Yee scheme as appears in [3] reproduced here to facilitate the understanding of how the source is implemented and the role each equation plays on the correction scheme.

For the electrical field $E_z^n(i,j)$, we have the following numerical scheme:

$$E_z^{n+1/2}(i,j) = E_z^{n-1/2}(i,j) + \frac{\Delta t}{\varepsilon_0 \mu_0 \Delta x}\left[B_y^n(i+1/2,j) - B_y^n(i-1/2,j)\right] - \frac{\Delta t}{\varepsilon_0 \mu_0 \Delta y}\left[B_x^n(i,j+1/2) - B_x^n(i,j-1/2)\right] \tag{4}$$

and an half time step latter the magnetic fields $B_x^n(i,j)$ and $B_y^n(i,j)$ are updated:

$$\begin{aligned} B_x^{n+1}(i,j+1/2) &= B_x^n(i,j+1/2) - \frac{\Delta t}{\Delta y}\left[E_z^{n+1/2}(i,j+1) - E_z^{n+1/2}(i,j)\right], \\ B_y^{n+1}(i+1/2,j) &= B_y^n(i+1/2,j) + \frac{\Delta t}{\Delta x}\left[E_z^{n+1/2}(i+1,j) - E_z^{n+1/2}(i,j)\right]. \end{aligned} \tag{5}$$

The propagation inside a guiding structure, albeit not being a free-space propagation, the fact of not having a physical medium inside the waveguide/antenna allows the use of the same set of equations. The walls of the guiding structure are implemented by setting the tangential electric field E_z to zero. In Fig. 1, we show the application of the scheme inside a waveguide section. With an usual hard source point, the excitation would be applied to the point $E_z(i_s,j_s)$. With the *hard line source* we excite the complete mode (usually TE_{10}) in the waveguide transversal section at i_s. The expression of the TE_{m0} excitation is

$$E_{z_{m0}}(i_s,j_s,t) = E_z(i_s,j_s,t)\sin\left[\frac{m\pi}{w_{wg}}(j-j_{-w})\right], \quad j_{-w} \leqslant j_s \leqslant j_{+w}, \tag{6}$$

where m is the index of the mode, j_{-w} and j_{+w} are the positions of electrical field before the waveguide walls and $w_{wg} = j_{+w} - j_{-w} + 1$ the waveguide width. $E_z(i_s,j_s,t) = E_{z_{m0}}(t)$ gives the evolution of the mode as a function of time, that is, what sort of signal we are exciting (frequency modulated, amplitude modulated, etc.). The injected signal via UTS can also be a sum of modes, which can be changed in time. Once excited, the field on line i inside the guide is propagated by the scheme forwards (exit of the waveguide/antenna) and backwards (border of the box) where it is absorbed by a boundary condition, in our case a perfectly matched layer (PML) [7]. Our goal is to obtain a excitation method were only a forward wave is excited.

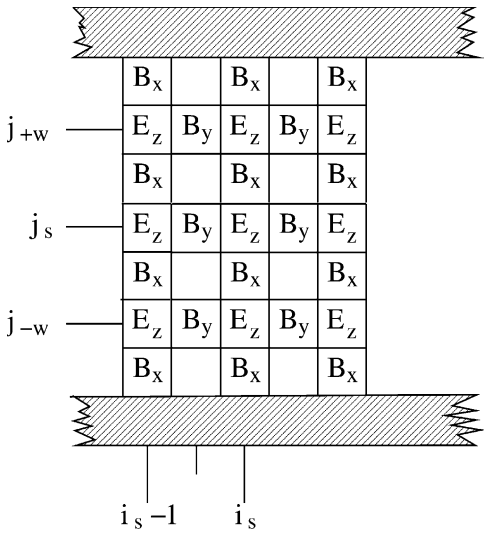

Fig. 1. Waveguide section showing the cells of the FDTD scheme.

2.2. Code solving the wave equation

Another approach to describe wave propagation in a vacuum is to solve the wave equation [24]. Combining Eqs. (1) and (4) assuming the transversal mode of propagation ($\mathbf{k} \perp \mathbf{E}$), we can easily obtain

$$\left(\frac{\partial^2}{\partial t^2} - c^2\nabla^2\right)\mathbf{E}_z(\mathbf{r},t) = \mathbf{0}. \tag{7}$$

For 2D propagation in the xy-plane (and the electric field polarized along the z-axis, $\mathbf{E}_z = E_z\mathbf{u}_z$), this equation gives

$$\left(\frac{\partial^2}{\partial t^2} - c^2\frac{\partial^2}{\partial x^2} - c^2\frac{\partial^2}{\partial y^2}\right)\mathbf{E}_z(\mathbf{r},t) = \mathbf{0}. \tag{8}$$

Using a second-order centered finite difference scheme, the second derivatives of Eq. (8) can be sampled as follows:

$$\begin{aligned}
\frac{\partial^2 E_z}{\partial t^2} &= \Delta t^{-2}\left[E_z^{n+1}(i,j) - 2E_z^n(i,j) + E_z^{n-1}(i,j)\right],\\
\frac{\partial^2 E_z}{\partial x^2} &= \Delta x^{-2}\left[E_z^n(i+1,j) - 2E_z^n(i,j) + E_z^n(i-1,j)\right],\\
\frac{\partial^2 E_z}{\partial y^2} &= \Delta y^{-2}\left[E_z^n(i,j+1) - 2E_z^n(i,j) + E_z^n(i,j-1)\right].
\end{aligned} \tag{9}$$

From Eqs. (8) and (9), we obtain the following expression for the electric field $E_z^n(i,j)$:

$$E_z^{n+1}(i,j) = \tfrac{1}{2}\left[E_z^n(i+1,j) + E_z^n(i-1,j) + E_z^n(i,j+1) + E_z^n(i,j-1)\right] - E_z^{n-1}(i,j). \tag{10}$$

To insure stability of the code, we have set $c^2\Delta t^2/\Delta x^2 = c^2\Delta t^2/\Delta y^2 = 1/2$. Iterative computations allow then evaluating the wave propagation in the grid. Transparent conditions as proposed in [25] have been input in the code to reduce parasitic reflections at the mesh boundaries [24].

The signal is injected as in the FDTD code (cf. Section 2.1). The source is then modeled by Eq. (6).

3. Principle of the unidirectional scheme

Let us first consider the waveguide topology depicted in Fig. 2 where a transverse mirror wall is placed at position $i_s - 1$ *before* the injection source line position i_s. Obviously all fields at positions with $i < i_s$ are zero and the excited electrical field propagates only in one direction. At positions with $i \geqslant i_s$ the fields have the behavior we are looking for on our unidirectional scheme, provided no reflected wave returns to the waveguide/antenna structure. Our aim is to excite this field structure without the mirror wall, allowing for the propagation of reflected waves at positions $i < i_s$, free of the main excited field.

3.1. Correction for FDTD Maxwell code

Supposing the mirror wall is kept up to instant $n - 1/2$ when it is removed, allowing the fields to propagate freely to positions $i < i_s$. At the next instant $n + 1/2$, we will have an electric field E_z at $i = i_s - 1$.

$$E_z^{n+1/2}(i_s - 1, j) = \frac{\Delta t}{\varepsilon_0\mu_0\Delta y}B_y^n(i_s - 1/2, j). \tag{11}$$

This expression is obtained from Eq. (4) applied to $i = i_s - 1$ taking into account that all the fields for $i < i_s$ are zero. If at this instant, we subtract the field $E_z^{n+1/2}(i_s - 1, j)$ to the field positions at $i = i_s - 1$ we reinstate

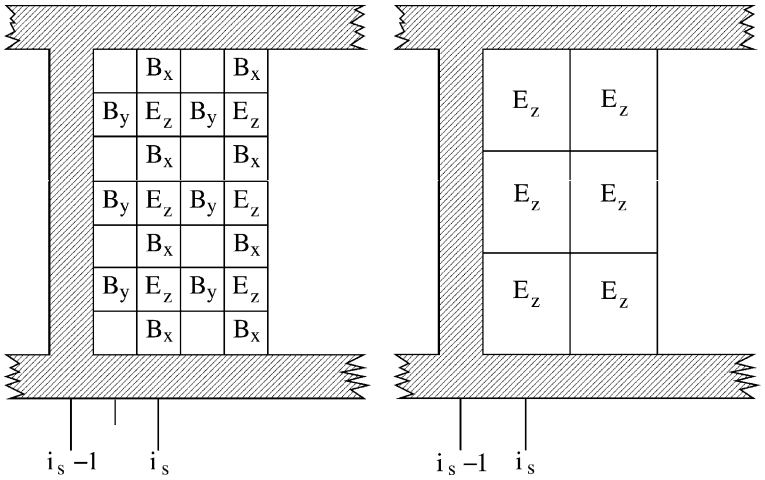

Fig. 2. Waveguide section showing the injection point with a reflecting wall (mirror) at left ($i_s - 1$) of the injection (i_s) for the FDTD Maxwell (left) and FDTD wave equation (right) schemes.

the situation we had before, that of null fields at $i < i_s$. The next B_x, B_y, half step, and E_z, a step latter, will have the same shape we would have, had we kept the mirror wall, with one important difference: the correction removes only the field due to the source. Any other field, coming from a reflected return signal, for instance, will not be altered and *transparently* will pass through the *correction barrier point* at i_s propagating for positions $i < i_s$ where it is isolated from the probing signal. The magnetic field $B_x(i - 1/2,j)$ obtained at n with the condition of $E_z(i_s - 1) = 0$ up to $n-1/2$ is our correction field at $n + 1/2$ (see Eq. (11)). If at each electric field stepping we make this correction, the exact cancellation of $E_z(i_s - 1,j)$ is performed and the unidirectional transparent injection scheme is kept working.

3.2. Correction for the FDTD wave-equation code

The principle of the method to obtain an unidirectional scheme in the wave equation code is similar to the one used for the FDTD Maxwell code as illustrated in Fig. 2. The residual electric field at the mirror position (given by Eq. (11)) becomes in the case of the wave equation code

$$E_z^{n+1}(i_s - 1, j) = \frac{c^2 \Delta t^2}{\Delta x^2} E_z^n(i_s, j). \tag{12}$$

4. Correction fields computation

We will briefly discuss the concepts of impulse response (IR) of a linear time-invariant system (LTI) [26], [27] and how these concepts are used to obtain the correction fields for the Maxwell (B_y) and wave-equation codes (E_z).

4.1. Impulse response of a linear time-invariant system

A system or an operator $\mathscr{T} : x \mapsto y$ is said to be linear if

$$\mathscr{T}\{ax_1 + bx_2\} = a\mathscr{T}\{x_1\} + b\mathscr{T}\{x_1\}. \tag{13}$$

If it furthermore verifies

$$\mathscr{T}\{x(t-t_0)\} = (\mathscr{T}\{x\})(t-t_0), \tag{14}$$

the system is also time-invariant.

The linear property means that the system follows the principle of *superposition* (additivity and homogeneity) and the time invariance means that the characteristics of the system remain unchanged in time. Systems verifying Eqs. (13) and (14) are called linear time-invariant systems (LTI) and are fully characterized by their impulse response $h(t)$

$$h(t) = \mathscr{T}\{\delta(t)\}, \tag{15}$$

where $\delta(t)$ the Dirac *function*. In the case of a discrete system

$$h[n] = \mathscr{T}\{\delta[n]\}, \tag{16}$$

where $\delta[n]$ is the unitary impulse defined as

$$\delta[n] = \begin{cases} 1 & \text{if } n = 0, \\ 0 & \text{otherwise.} \end{cases} \tag{17}$$

Note that n is equal to zero at the origin of the discrete times.

Any function $x[n] = f[n] = f(n\Delta t)$ can be written as

$$x[n] = \sum_{k=-\infty}^{+\infty} f(k\Delta t)\delta[n-k]. \tag{18}$$

Since the system is LTI, its output is

$$y[n] = \sum_{k=-\infty}^{+\infty} f(k\Delta t)h[n-k]. \tag{19}$$

Systems whose impulsive response are finite are known as finite impulsive response (FIR) systems. If the impulsive response is infinite they are called infinite impulsive response (IIR) systems. The amplitude of the impulsive response of a IIR system asymptotically decreases to zero (conservation of energy) and eventually drops below the noise level of the system. From this point onwards, the remaining samples can (and should) be ignored since they do not contribute to the response of the system but add noise to the computation. The choice of the number of samples to consider when dealing with an IIR influences the accuracy of the system response. Depending on the required level of accuracy the number of samples can be less than the one imposed by the noise level of the system.

Since we are interested in causal systems and the number of samples N of the impulsive response considered is finite (because the system is a FIR or we chose a cutting criterion for an IIR) the output of the system can be simplified to

$$y[n] = \sum_{k=0}^{N-1} f(k\Delta t)h[n-k] + \epsilon[n], \tag{20}$$

where $\epsilon[n]$ is the error in the evaluation of $y[n]$.

4.2. Excitation signals

According to the selected signal $f(t)$, different types of reflectometers [1] can be simulated, although from the point of view of the unidirectional transparent injection the problem (and solution) is the same. In our simulations, we deal usually with continuous wave fixed frequency (CWFF)

$$E_{z_s}(t) = A_i \cos(\omega_0 t + \varphi_0), \tag{21}$$

and CWFM. The frequency modulated (FM) signal has an instantaneous frequency [28] $f(t) = f_c + f_\Delta g(t)$, with $f_\Delta < f_c$, where f_Δ is the frequency deviation, f_c the carrier frequency, and $g(t)$ the modulating signal, in our case a ramp. The instantaneous frequency of the signal varies from a minimum frequency $f_m = f_c$ to a maximum frequency $f_M = f_c + f_\Delta$ during the interval of a sweep T_s. The input FM signal is

$$E_{z_s}(t) = A_i \cos\left[\omega_c t + 2\pi f_\Delta \int^t g(\lambda)\, d\lambda\right]. \tag{22}$$

Other types of signal have been excited with the UTS, namely modulated Gaussian (pulse reflectometry) and amplitude modulation (AM) when simulating these types of reflectometry experiments.

4.3. Impulsive response of a 1D mirrored waveguide

Although our main goal is to implement an UTS in a 2D waveguide, we present 1D cases to demonstrate in a simple way the principle of using the impulsive response of the system as the correction field needed to guarantee the unidirectional transparent signal injection. The case of *1D mirrored waveguide* is obviously just a point where total reflection is imposed (*mirror*) in order to obtain the impulsive response (see Fig. 3). We adopt the 2D terminology to facilitate the analogy with the 2D case which is dealt with in Section 4.4.

In this section, we present two cases: a *waveguide* in a vacuum and a *waveguide* filled with an homogeneous dielectric medium, such as an homogeneous plasma.

The input in the 1D system is the electric field E_z at $i = i_s$ and the output, the magnetic field B_y at $i = i_s - 1/2$. In the 1D case, the magnetic field equation (5) simplify to one equation for B_y

$$B_y^{n+1/2}(i_s - 1/2) = \frac{\Delta t}{\Delta x} E_z^n(i_s). \tag{23}$$

In the following, we prove that such a system is LTI. Since for a given $n = N$, the output depends on the fields at instants $n < N$ we prove our statements for $n = 0$ (first time instant) and for an arbitrary N. By induction our assertion is valid at all instants n.

For $n = 0$ if we have

$$B_{y_1}^{(1/2)} = \frac{\Delta t}{\Delta x} E_{z_1}^0,$$

$$B_{y_2}^{(1/2)} = \frac{\Delta t}{\Delta x} E_{z_2}^0$$

then for an input $E_z^0 = aE_{z_1}^0 + bE_{z_2}^0$ we will have an output

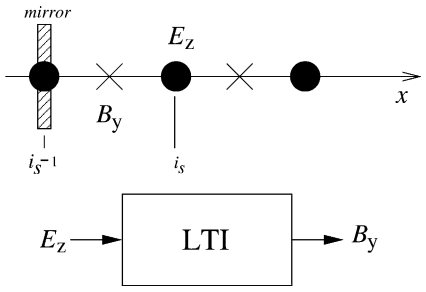

Fig. 3. 1D mirrored waveguide as a LTI system.

$$B_y^{(1/2)} = \frac{\Delta t}{\Delta x} E_z^0 = \frac{\Delta t}{\Delta x}(aE_{z_1}^0 + bE_{z_2}^0) = \frac{\Delta t}{\Delta x} aE_{z_1}^0 + \frac{\Delta t}{\Delta x} bE_{z_2}^0 = aB_{y_1}^{(1/2)} + bB_{y_2}^{(1/2)},$$

that is linearity (*superposition*) is verified at $n = 0$. Assuming that linearity is verified for $n = N - 1$, then at $n = N$ if

$$B_{y_1}^{(N+1/2)} = \frac{\Delta t}{\Delta x} E_{z_1}^N,$$
$$B_{y_2}^{(N+1+2)} = \frac{\Delta t}{\Delta x} E_{z_2}^N$$

then for a $E_z^N = aE_{z_1}^N + bE_{z_2}^N$, we obtain

$$B_y^{(N+1/2)} = \frac{\Delta t}{\Delta x} E_z^N = \frac{\Delta t}{\Delta x}(aE_{z_1}^N + bE_{z_2}^N) = \frac{\Delta t}{\Delta x} aE_{z_1}^N + \frac{\Delta t}{\Delta x} bE_{z_2}^N = aB_{y_1}^{(N+1/2)} + bB_{y_2}^{(N+1/2)}.$$

By induction, it is established that the system is linear.

The system is also time invariant since the relations between the fields do not depend on time. The system is then a LTI and the impulsive response technique can thus be applied.

With the knowledge of B_y the correction of the electric field at the *mirror* position $i = i_s - 1$ can be made numerically without having to enforce it to null. This correction, apart from being unidirectional, will also be transparent to the incoming wave. The corrective field for the 1D case is

$$E_z^{n+1/2}(i_s - 1) = \frac{\Delta t}{\varepsilon_0 \mu_0 \Delta y} B_y^n(i_s - 1/2). \tag{24}$$

Exciting the system with unitary impulse $E_z^n(i_s) = \delta[n]$ the impulsive response of the system $h[n] = B_y^{n+1/2}$ is obtained. Fig. 4 displays the impulsive response for 1D FDTD Maxwell scheme when $\Delta x/\Delta t = c$, condition known as the *magic step* [23] since no numerical dispersion is present in the code results. This system is a FIR.

If we change the relation $\Delta x/\Delta t$ to a different value a new LTI system, different from the former, is obtained and its impulsive response is consequently distinct. In Fig. 5, the impulsive response for $\Delta x/\Delta t = 0.5c$ is depicted. We face clearly a system different from the one presented in Fig. 4. The fact that the code is not being run with the magic step implies the existence of numerical dispersion and consequently all frequencies contribute with different propagation velocities to the system response (note that an unitary impulse corresponds to a constant level in the frequency space). This emphasizes the fact that when a change on the LTI system (FDTD code) is done, a new system with a new impulsive response (new corrective field) is obtained.

If the propagation is not in vacuum (e.g., for a dielectric filled waveguide) the corrective field is no more given by Eq. (24). With the addition of an homogeneous plasma, the corrective field is given by

$$E_z^{n+1/2}(i_s - 1) = \frac{\Delta t}{\varepsilon_0 \mu_0 \Delta y} B_y^n(i_s - 1/2) - \frac{\Delta t}{\varepsilon_0} J_z^n(i_s - 1/2). \tag{25}$$

There is an extra term appearing in the corrective field now, the current density which accounts for the plasma effects. This term must also be known in order to correct the injection using the impulsive response technique. The system, with input $x[n] = E_z^n(i_s)$ has now as output a vector

$$\mathbf{Y}[n] = \left(B_y^{n+1/2}(i_s - 1/2), J_z^{n+1/2}(i_s - 1/2)\right).$$

Following a procedure similar to the one used previously, this new system can be proved to be LTI. When excited with an unitary impulse $E_z^n(i_s) = \delta[n]$, the impulsive response of the system is obtained as $\mathbf{H}[n] = (h_B[n], h_J[n])$.

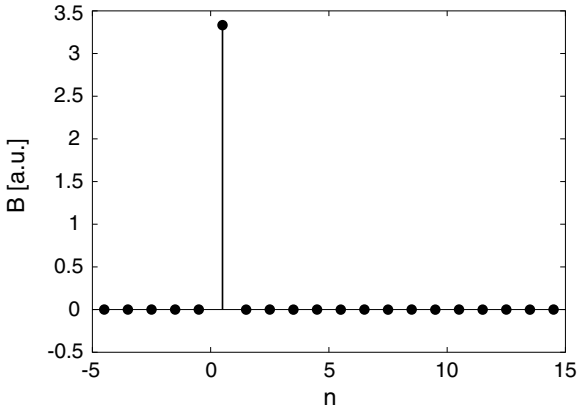

Fig. 4. Impulsive response of a 1D *mirrored* FDTD Maxwell code with $\Delta x/\Delta t = c$ (*magic step*).

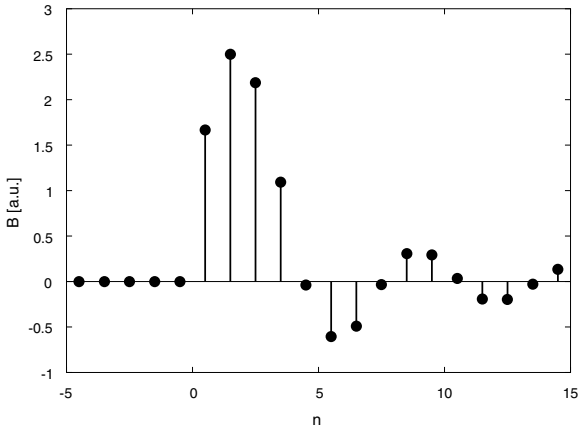

Fig. 5. Impulsive response of a 1D *mirrored* FDTD Maxwell code with $\Delta x/\Delta t = 0.5c$.

In Fig. 6, the two components, $h_B[n]$ and $h_J[n]$, of the impulsive response $\mathbf{H}[n]$ for a 1D *waveguide* filled with a constant homogeneous plasma with a plasma frequency $f_{pe} = 30$ GHz are shown. Although the *magic step* is used ($\Delta x/\Delta t = c$), the presence of the plasma introduces physical dispersion on the system.

4.4. Impulse response of the 2D mirrored waveguide

To obtain the corrective field $B_y(i_s - 1/2,j)$, we will use the structure presented in Fig. 2 for the LTI system. The input of the system is a vector whose components are the values of the electric field $E_z(i_s,j)$ in the line $j_{-w} \leqslant j \leqslant j_{+w}$ at $i = i_s$.

$$\mathbf{X}[n] = \left(E_z^n(i_s, j_{-w}), \ldots, E_z^n(i_s, j_0), \ldots, E_z^n(i_s, j_{+w})\right) \tag{26}$$

and the output, a vector whose components are the values of the magnetic field B_y in the line $j_{-w} \leqslant j \leqslant j_{+w}$ at $i = i_s - 1/2$ for the FDTD Maxwell code.

$$\mathbf{Y}[n] = \left(B_y^n(i_s - 1/2, j_{-w}), \ldots, B_y^n(i_s - 1/2, j_{+w})\right).$$

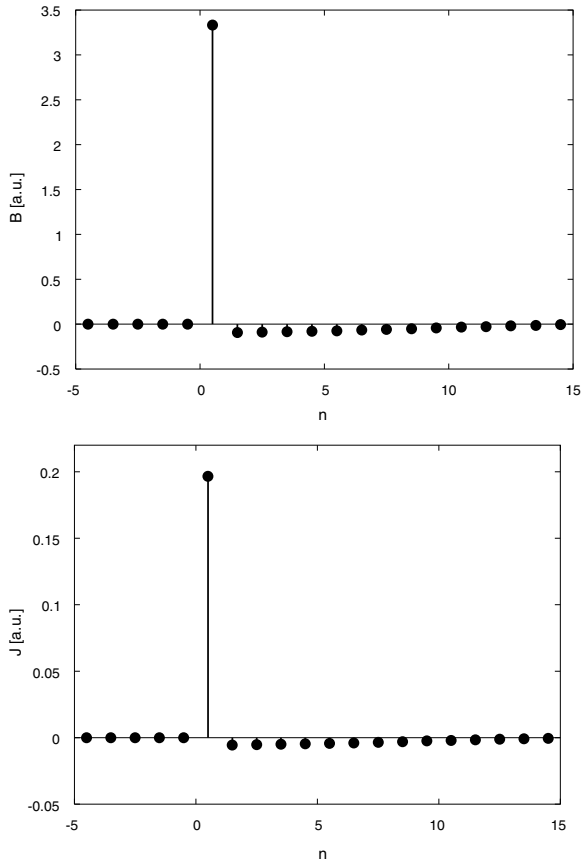

Fig. 6. Impulsive response $\mathbf{H} = (h_B[n], h_J[n])$ of the 1D plasma filled *waveguide*.

Each of the components $Y_j[n]$ of $\mathbf{Y}[n]$ is a function of all components of $\mathbf{X}[n]$, that is $\mathbf{X} \mapsto Y_j$. The output $\mathbf{Y}$ can be thought as an *array* of individual LTI systems of vectorial input $\mathbf{X}$ and output Y_j.

A system with multiple inputs is linear if it is a combination of linear subsystems and additions of signal [27]. By placing a signal on an input while the others are held to zero a response is obtained for the output. Repeating the procedure for other inputs new responses are obtained at the output. When forcing all the inputs with the test signals previously used, the output is the sum of the partial outputs.

An analysis of the set of equations (4) and (5) (see also Fig. 2) shows that an output $Y_k[B_y(i_s - 1/2, k)]$ depends on the input *in front* $X_k[E_z(i_s, k)]$ in the same way as the 1D system presented in Section 4.3 (see Eq. (23)), when all other inputs are set to zero. Another input X_j^n with $j \neq k$ at instant n is propagated by the FDTD scheme until it reaches the position k scaled by a_j and with a delay N_j, that is as a new input $X_{k(j)}^n = a_j X_j^{n-N_j}$, resulting in a new output $Y'_{k(j)}$. With all inputs present, X_k^{tot} will be a sum of all contributions

$$X_k^{tot} = X_k^n + \sum_{j,j\neq k}^{J-1} X_{k(j)}^n = X_k^n + \sum_{j,j\neq k}^{J-1} a_j X_j^{n-N_j}.$$

Since the linear subsystem $(X_k \mapsto Y_k)$ satisfies the superposition principle, the overall system $\mathbf{X} \mapsto Y_k$ is linear.

The system is also time invariant since relations between the fields do not depend on time. The system is then a LTI and the impulsive response technique can thus be applied.

For the FDTD wave-equation the output is

$$\mathbf{Y}[n] = \left(E_z^n(i_s - 1, j_{-w}), \ldots, E_z^n(i_s - 1, j_{+w})\right).$$

The term vector used in the previous paragraph does not refer to the electric and magnetic vector fields in the sense of electromagnetic entities but in the sense of *multicomponent* input and output of the LTI system (see Fig. 7). To obtain the impulsive response of the system, we excite it with an *impulse vector* $\mathbf{\Delta}[n]$,

$$\mathbf{\Delta}[n] = \delta[n] \quad \text{for } i = i_s, j_{-w} \leqslant j \leqslant j_{+w}. \tag{27}$$

The response of the system to the impulse vector

$$\mathbf{H}[n] = \mathscr{T}\{\mathbf{\Delta}(t)\} \tag{28}$$

describes the *mirrored* waveguide system and can be used to obtain the output to an excitation (e.g., as given by Eq. (6)). Defining as input

$$\mathbf{X}[n] = \left(\ldots, E_{z_s}^n(i_s, j), \ldots\right) \quad \text{with } j_{-w} \leqslant j \leqslant j_{+w}, \tag{29}$$

we have as output

$$\mathbf{Y}[n] = \left(\ldots, \sum_{k=-\infty}^{+\infty} X_j[n] H_j[n-k], \ldots\right) \quad \text{with } j_{-w} \leqslant j \leqslant j_{+w}, \tag{30}$$

where $X_j[n]$ and $H_j[n]$ are the jth components of the vectors $\mathbf{X}[n]$ and $\mathbf{H}[n]$ (in the LTI sense).

In Fig. 8, the impulsive response for the FDTD Maxwell code is depicted.

A waveguide, being a dispersive component, propagates the frequency components of $\Delta[n]$ at different velocities. The UTS source has no problem with this type of signal and describes well an excitation of a Dirac pulse train.

4.5. Evaluation of the number of coefficients

In this section, we discuss the number of coefficients to be used for an evaluation with a known (low) error of the electric field E_z at $i = i_s - 1$ (cf. Eqs. (11) and (12)).

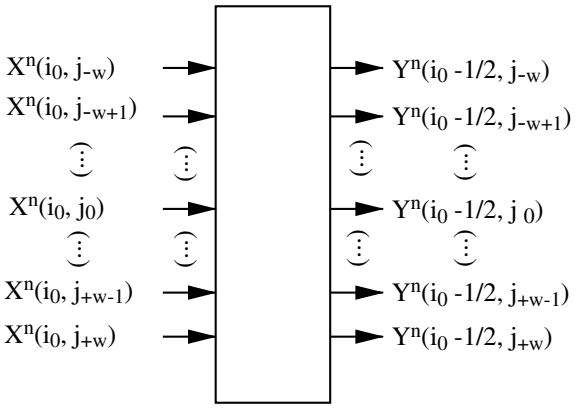

Fig. 7. LTI system schematic for the 2D mirrored waveguide. The input $\mathbf{X}$ is the electric field at $(i_s, j_{-w} \leqslant j \leqslant j_{+w})$ and the output $\mathbf{Y}$ is the magnetic field at $(i_s - 1/2, j_{-w} \leqslant j \leqslant j_{+w})$ for FDTD Maxwell code or the electric field at $(i_s - 1, j_{-w} \leqslant j \leqslant j_{+w})$ for the wave equation code.

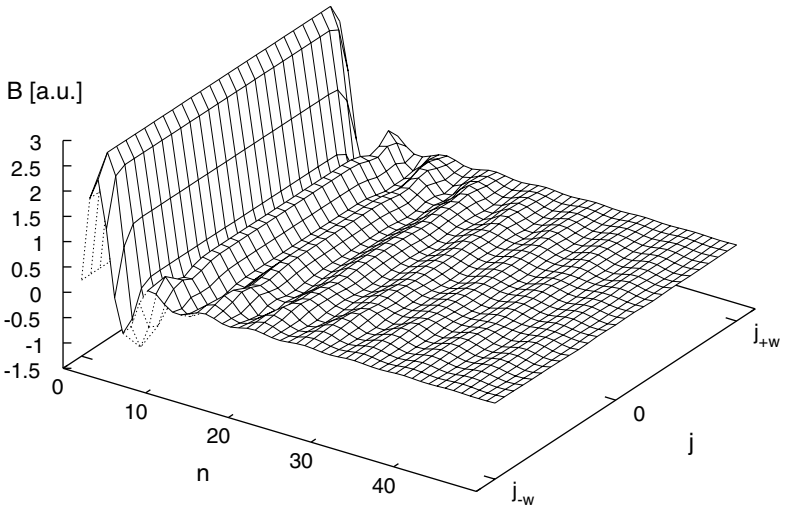

Fig. 8. Impulse response $\mathbf{Y}[n]$ of the 2D *mirrored* waveguide FDTD Maxwell code (first 50 time steps).

4.5.1. Analytical evaluation for simplified version of the UTS

We consider the case of the wave equation code but this discussion remains valid for the FDTD Maxwell code. From Eqs. (12) and (30), the electric field E_z at $i = i_s - 1$ to be corrected can be written as follows:

$$E_z^{n+1}(i_s - 1, j) = \frac{c^2 \Delta t^2}{\Delta x^2} \sum_{k=0}^{+N_{coef}} E_z^{n-k}(i_s, j) \tag{31}$$

where N_{coef} is the number of coefficients used for the correction. Ideally contributions from all previous times, from $t = 0$ up to $t = n\delta t$, should be taken into account and therefore N_{coef} should be set equal to n. For a high number of iterations, this would induce long times of computations. Moreover since the contribution from $E_z^{n-k}(i_s, j)$ decreases when k drops to n, we show that the value of N_{coef} can be optimized.

For simplicity, we assume now that the source emits a fixed frequency f in a TM_{10} mode. Then we can write:

$$E_z^{n-k}(i_s, j) = \cos\left[\frac{\pi}{w_{wg}}(j - j_{-w})\right] \cos\left[2\pi(n-k) f \delta t\right]. \tag{32}$$

For this particular case, Eq. (31) can be then expressed as:

$$E_z^{n+1}(i_s - 1, j) = \frac{c^2 \Delta t^2}{\Delta x^2} \cos\left[\frac{\pi}{w_{wg}}(j - j_{-w})\right] \sum_{k=0}^{+N_{coef}} \cos\left[2\pi(n-k) f \delta t\right]. \tag{33}$$

That is, assuming $t = n\delta t$:

$$E_z^{n+1}(i_s - 1, j) = \frac{c^2 \Delta t^2}{\Delta x^2} \cos\left[\frac{\pi}{w_{wg}}(j - j_{-w})\right] \sum_{k=0}^{+N_{coef}} \cos\left[2\pi f (t - k\delta t)\right]. \tag{34}$$

From Eq. (34), $E_z^{n+1}(i_s - 1, j)$ appears clearly as a sum of waves at the same frequency shifted by a phase $2\pi f k \delta t$. Consequently, we can write this field to be corrected as:

$$E_z^{n+1}(i_s - 1, j) = A \cos\left[2\pi f t - \phi\right], \tag{35}$$

where A and ϕ are given respectively by:

$$A = \frac{c^2\Delta t^2}{\Delta x^2}\cos\left[\frac{\pi}{w_{\mathrm{wg}}}(j - j_{-\mathrm{w}})\right] \times \left\{\left[\sum_{k=0}^{+N_{\mathrm{coef}}} \cos(2\pi f k\delta t)\right]^2 + \left[\sum_{k=0}^{+N_{\mathrm{coef}}} \sin(2\pi f k\delta t)\right]^2\right\}^{1/2}, \tag{36}$$

$$\phi = \arctan\left[\frac{\sum_{k=0}^{+N_{\mathrm{coef}}} \sin(2\pi f k\delta t)}{\sum_{k=0}^{+N_{\mathrm{coef}}} \cos(2\pi f k\delta t)}\right]. \tag{37}$$

Values of the amplitude and phase of $E_z^{n+1}(i_s - 1, j)$, given by Eqs. (36) and (37) as a function of the number of coefficients N_{coef} are displayed in Fig. 9. This figure confirms that A and ϕ seem to converge so that they can be assumed constant above a given value of the coefficient number N_{coef}. In other terms, it means that the UTS source reaches a stationary regime after a given time. Then, the number of coefficients N_{coef} has to be chosen high enough to reach the stationary regime where the amplitude A and the phase ϕ can be assumed constant. This is exemplified in Fig. 10 where an evaluation of the electric field $E_z^{n+1}(i_s - 1, j)$ is made using $N_{\mathrm{coef}} = 10$ and $N_{\mathrm{coef}} = 300$. For $N_{\mathrm{coef}} = 10$, the evaluation of $E_z^{n+1}(i_s - 1, j)$ is not accurate as the phase A and amplitude ϕ cannot be considered constant. Then, the correction of $E_z^{n+1}(i_s - 1, j)$ is not sufficiently efficient to prevent emission of the wave in the backward direction. For $N_{\mathrm{coef}} = 300$, A and ϕ can be assumed equal to their respective asymptotic values. We can notice that the undesired backward emission of the wave is almost removed. A compromise has to be found between fast computations (for low N_{coef}) and an accurate directive emission (for high N_{coef}).

4.5.2. Implementation of the UTS source in a closed waveguide

The 2D FDTD Eqs. (4) and (5) were solved on a computation grid where the waveguide was modeled imposing the tangential electric field to null on the waveguide walls, $E_z = 0$ (Fig. 12(a)). The extremities of the waveguide are *closed* with a perfectly matched layer (PML) [7]. To obtain the impulsive response the mirror, as described in Section 3 (see Fig. 2), is also done imposing $E_z = 0$. An impulse $\mathbf{\Delta}[n]$ is applied at i_s and its output $\mathbf{H}[n]$ recorded. The length of the waveguide is chosen so that the recorded length of its impulsive response (number of recorded samples) does not have any spurious return from the PML. Although PML conditions are quite efficient, the fact that we are in a close waveguide means that the

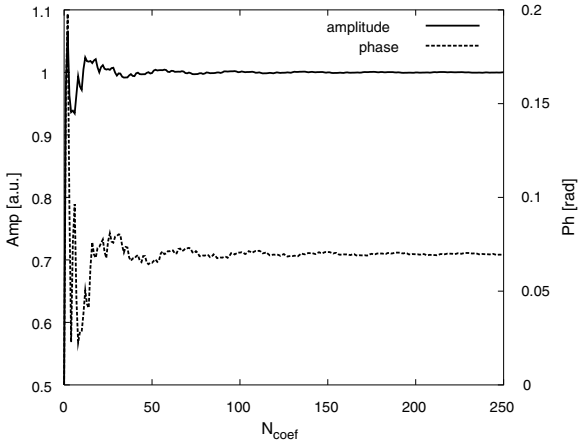

Fig. 9. Amplitude and phase of $E_z^{n+1}(i_s - 1, j)$ as a function of N_{coef} in a vacuum.

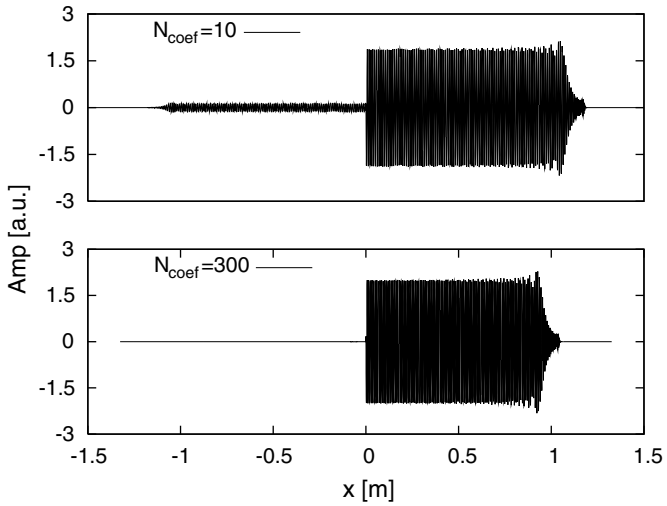

Fig. 10. Cut in the waveguide axis of a directive wave emission respectively with 10 and 300 coefficients used. Field amplitude is chosen to give unitary amplitude in a vacuum.

PML receives all of the *energy* excited in the guide on a narrow width and the parasitic reflection, even marginal, may have a magnitude comparable to the samples of higher n (which have very low amplitude).

With the knowledge of the impulsive response $\mathbf{H}[n]$ the *calibration* mirror can be removed and with the corrective field obtained from Eq. (30) the correction stated by Eq. (11) applied. An UTS is thus implemented.

4.5.3. Numerical performance of the UTS versus the number of coefficients

As shown in Section 4.5.2, the number of coefficients considered N_{coef} in the correction of of the source influences the accuracy of the correction. Due to the finite number of coefficients used in the UTS to inject the TE_{10} mode, spurious TE_{m0} modes are also excited despite having a low amplitude. In Fig. 11 the ratio

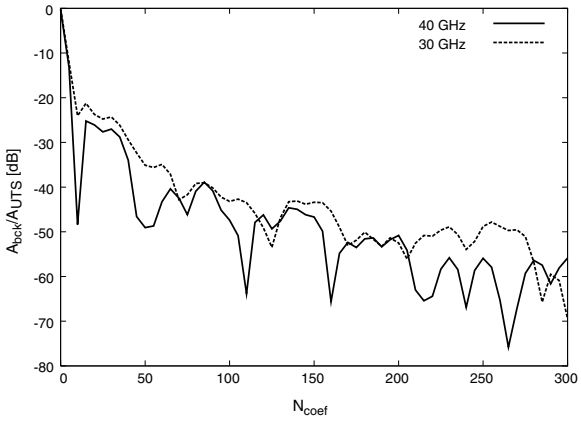

Fig. 11. Ratio between the residual backward signal amplitude A_{bck} and the amplitude of the *direct* source signal A_{UTS} as a function of the number of coefficients, N_{coef}, of the IR used.

between the amplitude A_{bck} of the residual back-propagating signal (taken at $i_s - 1$) and the amplitude of the *direct* source signal A_{UTS} (taken at i_s) is shown as a function of the number of samples (N_{coef}) used for correction for two excitation frequencies $f = 30$ GHz and $f = 40$ GHz. On the simulations presented on this paper, we have considered a spatial discretization of $\Delta x = \Delta y = \lambda_{40\ GHz}/20$ and a temporal discretization of $\Delta t = T_{40\ GHz}/40$. The waveguide (see Fig. 12(a)) is made sufficiently long so that no return from the closing PML might interfere with the input wave. From a certain number of correction terms, it can be noticed that the average level of the correction stabilizes. The cyclical wells in the curves occur at cut-off frequencies for the residual TE_{m0} modes, with a very low amplitude, spuriously induced in the waveguide with the main signal. When the number of correction points, N_{coef}, equals the exact number of points of a complete mode period from a residual mode frequency a better compensation is obtained.

5. Implementation of the method in open emission structures. UTS characteristics

5.1. Implementation of the UTS on an open structure

Until now the implementation of the injection scheme was done on a closed waveguide (i.e., closed with PML boundary conditions) which is useful to simulate propagation in waveguides but does not yet meet our final goal of sending a probing wave towards a free-propagation zone. For that purpose we have to use an open radiating structure such as an open waveguide or an antenna as depicted in Fig. 12(b) and (c). These form LTI systems whose IR differ from the IR of the closed waveguide. Two approaches will follow: (1) to use the impulsive response of the closed waveguide and (2) to obtain the adequate IR for the new LTI system.

The open waveguide/antenna launches the signal to an open free-propagation zone or/and a media such as an inhomogeneous plasma. The computation box is surrounded by a PML boundary as well as the back section of the waveguide. With an open waveguide (Fig. 12(b)), using the same procedure as in Section 4.5.3, the ratio A_{bck}/A_{UTS} was evaluated. In Fig. 13, this ratio is presented for three values of L, the distance between the UTS and the *mouth* of the waveguide (see Fig. 12). The IR used to correct the source is the one

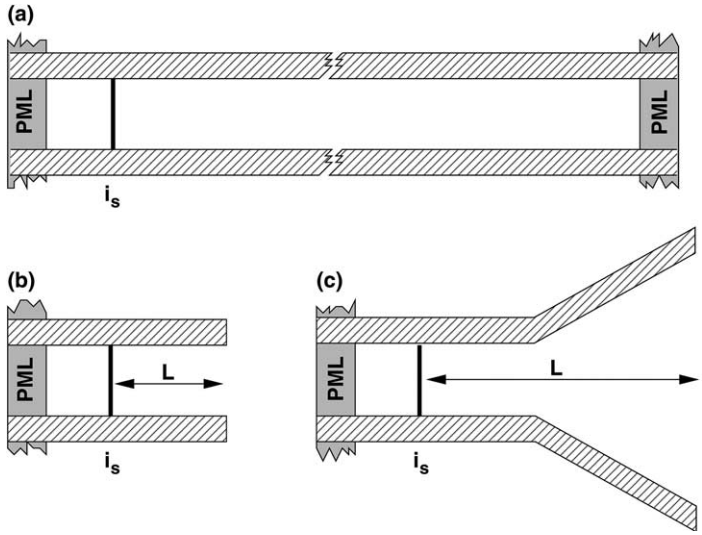

Fig. 12. Different structures of emission. (a) Closed waveguide, (b) open waveguide and (c) H-plane sectorial horn.

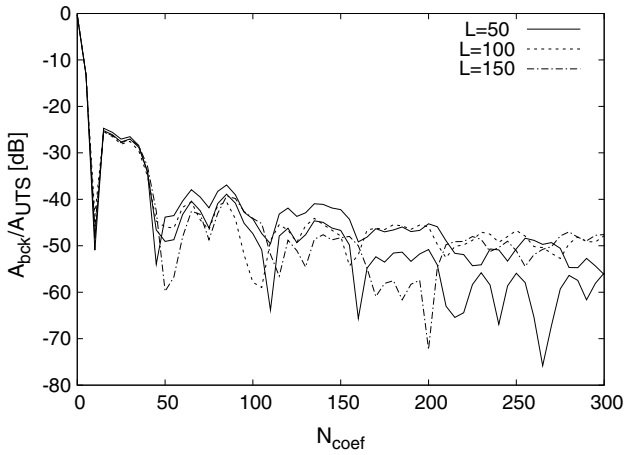

Fig. 13. Ratio between the A_{bck} and A_{UTS} for open waveguide using the IR for the closed waveguide as a function of the number of coefficients, N_{coef}. The response for the closed waveguide is shown as a reference by the thin continuous line for 40 GHz input frequency.

obtained for the closed waveguide. The differences between the obtained ratios highlight the differences between the two LTI systems. The wave traveling in open waveguide faces a sudden transition from guided propagation to open-space propagation, resulting in the reflection of part of the signal. This is a physical characteristic of the system, not a code feature.

For the horn antenna (Fig. 12(c)), the ratios A_{bck}/A_{UTS} are shown in Fig. 14. The IR of the closed waveguide was used in one test (IR = CWG) and in the other, the IR of the *antenna system* was evaluated and used in the correction (IR = HA).

We can notice in Figs. 13 and 14 that using the IR for the closed waveguide while working with an open structure does not introduce major differences in the correction level for $N_{coef} < 150$. This means that in

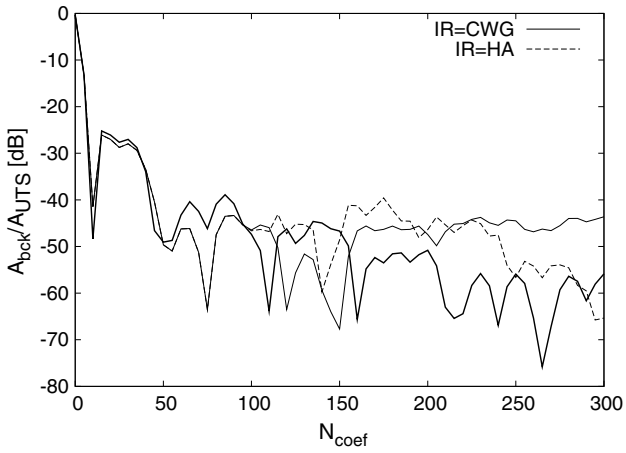

Fig. 14. Ratio between the A_{bck} and A_{UTS} for a sectorial horn antenna where the IR for the closed waveguide (IR = CWG) and for the antenna (IR = HA) are used as a function of the number of coefficients, N_{coef}, of the IRs used. The response for the closed waveguide is shown as a reference by the thin continuous line.

such conditions the initial length of the waveguide determines the main response of the system. For a same waveguide width, the same impulsive response can be used with the open structures. For a given calibration of A_{bck}/A_{UTS} in the limit of the numerical scheme accuracy, the number of coefficients N_{coef} can be *fine-tuned* following the dependencies shown in Figs. 13 and 14.

5.2. UTS characteristics

We look now into the characteristics displayed by our implementation of the UTS on a horn antenna.

5.2.1. Waveguide modes

Besides the type of signal injected by the source, the mode excited in the wave guide can also be selected. In Fig. 15, it is depicted the corrected emission for the TE_{10} and TE_{20} waveguide modes [cf. Eq. (6)] [29]. Note that the waveguide TE mode corresponds to a TM propagation mode.

5.2.2. Spectral characteristics of the 2D injection scheme

It is important to verify that the UTS does not change the usual spectral characteristics of the system and keeps the spectrum of the injected signal as pure as the *original* (uncorrected source) without introducing any spurious component. In Fig. 16, spectra are shown for a continuous wave fixed frequency (CWFF) signal for an UTS source and for an *uncorrected* source both emitting at $f_c = 40$ GHz. An excellent spectral purity is kept by the method with widths of $\Delta f/f_c = 0.009\%$ at 3 dB and $\Delta f/f_c = 0.04\%$ at 10 dB with more than 70 dB (more than ×3000) above the floor noise (high S/N ratio).

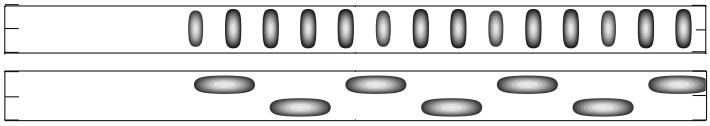

Fig. 15. TE_{10} and TE_{20} waveguide modes.

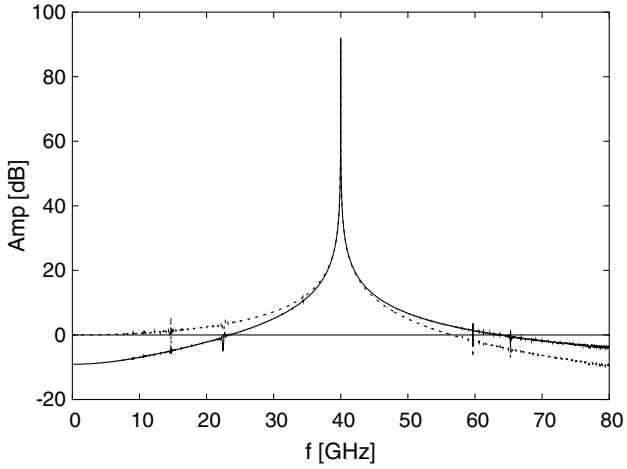

Fig. 16. Spectra of a CWFF UTS (continuous line) and an *uncorrected* sources emitting at $f = 40$ GHz (dashed line).

For a continuous wave frequency modulated (CWFM), the signal keeps also a good purity and separation from the floor noise.

5.2.3. Antenna characteristics

The proposed method of implementing an UTS makes use of both the signal injection scheme and the radiating structure (waveguide and antenna). Apart from keeping all the signal characteristics when implementing an UTS, the antenna characteristics should also remain unaltered. The emission diagram must be the same with or without the UTS and antenna reciprocity must be preserved. The emission diagrams for the H-plane sectoral horn antenna used on the simulations presented in Section (6.2) were calculated with and without an UTS. We have confirmed that the radiation pattern is not altered by the UTS. A test was also done by emitting a signal towards an UTS emitting antenna. The signal picked-up at the back of the source was compared with the signal picked-up from a *quiet* antenna (just the emitting structure) and no difference was observed, that is an emitting UTS does not alter the received signal. These tests assured that the UTS keeps the antenna characteristics.

6. Applications

Simulations showing the application of the method in 2D cases where performed on a $51\lambda_{40}$ GHz $\times$ $36\lambda_{40}$ GHz 2D computation grid, probing a linear plasma n_{e_0}, whose maximum value is $2.5 \times 10^{19}\mathrm{m}^{-3}$ ($f_{pe} = 45.0$ GHz) at $x = 33\lambda_{40\ \mathrm{GHz}}$. Simulations took 100,000 time steps (62.5 ns) each. Simulations of swept reflectometry (FMCW) covered a frequency range of [30–40] GHz (corresponding to a density range of $[1\text{–}2] \times 10^{19}$ m^{-3}). The plasma density is *damped* close to the box borders to match the vacuum propagation conditions suited to the Perfectly Matched Layer (PML) technique, used as a boundary condition. A single H-plane sectoral horn antenna, is used both for emission and reception (monostatic antenna). The feeding waveguide is excited with the fundamental mode TE_{10}. Density modes $\delta n_{e_{mod}}(t)$ and turbulence $\delta n_{e_{trb}}(t)$ may be added to the *unperturbed* plasma $n_{e_0} : n_e = n_{e_0} + \delta n_{e_{mod}} + \delta n_{e_{trb}}$.

6.1. Profile measurements – determination of the phase derivative

One of the main applications of reflectometry is electronic density profile measurement, done mainly with FMCW broadband reflectometry [1]. In the case of ordinary mode (O-mode) reflectometry, where the probing electric field is parallel to the external magnetic field, the reflection point is given by the equality between the plasma frequency $f_{pe} = 8.98 n_e^{1/2}$ (in SI units) and the probing frequency $f(t)$. Sweeping the frequency, the phase difference $\varphi(f)$ between the probing and the reflected waves can be obtained for a continuous range of frequencies (reflection locations) and a curve of the phase derivative $\partial\varphi/\partial f$ obtained. Using an Abel inversion is possible to reconstruct the plasma density profile (assuming monotonicity) [5]. The Abel inversion gives the distance $d(f)$ between the antenna and the cut-off position as a function of the phase derivative versus the probing frequency:

$$d(f) = \frac{c}{2\pi^2} \int_0^f \frac{\partial\varphi}{\partial f} \left(f^2 - v^2\right)^{-1/2} \mathrm{d}v, \tag{38}$$

where c is the speed of light in a vacuum.

It is therefore important to have direct access to the reflected wave in order to calculate the phase derivative. To extract the phase the returned and the reference signals are mixed (multiplied) resulting in a signal with low frequency and high frequency components. The high frequency component is filtered out. The resulting low frequency signal, containing the phase information, is called the reflectometry signal

$$s_{ref}(t) = A_s(t) \cos[\varphi(t)]. \tag{39}$$

From Eq. (39) the phase $\varphi(t)$ (and consequently $\partial\varphi/\partial f$) or the beat frequency f_B (and $\partial\varphi/\partial f = 2\pi(\partial f/\partial t)^{-1} f_B$) can be obtained using an appropriate signal processing technique. In the case presented here a sliding FFT is applied to obtain f_B. In Fig. 17 the return signal (reflected) obtained from the frequency sweep is shown together with the phase derivative $\partial\varphi/\partial f$. The modulation seen on the reflected signal comes from multi-reflexion between the horn and the plasma cut-off.

The evaluation of the phase difference between the emitted and returned signals, needed to reconstruct or evaluate the perturbations induced on the density profile although not impossible is more complicated with the presence of both signals (emitted and reflected) and more susceptible to numerical errors due to a low dynamic computation range and additional data processing.

6.2. Destructive interference simulation

Coherent density perturbations in a plasma can induce strong perturbations on the amplitude of the reflectometry signal and lead to destructive interference phenomena as shown in the following example. The use of an UTS is essential to a correct analysis of the destructive interference occurrence. If the plasma

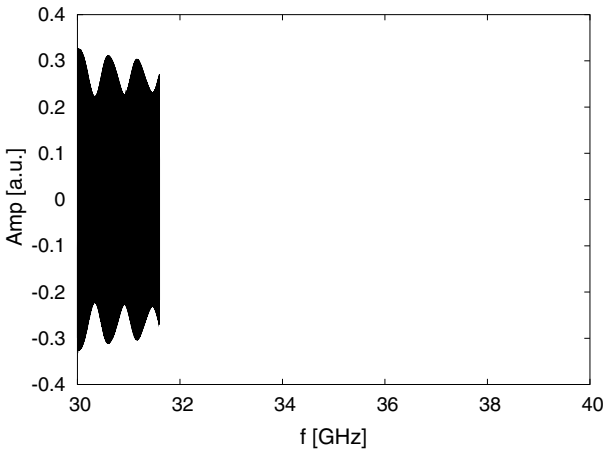

retu ed from much stronger emission signal, the interference signature is lost is modeled using

$$\sin [N_i k_m (y - y_i(t)) + \varphi_i]\}, \tag{40}$$

whe lar) wavenumber corresponding to the width of the calculation box (po in the box at a time, x_i the radial position of the chain, $w_x = 18.75$ m c magnetic island [30,31], $A_f = 3.5 \times 10^{18}$ m^{-3} is the amplitude of the isla lly at $x_{c_{35}} = 31.2\lambda_{40\ \mathrm{GHz}}$ (the cut-off position for $f = 35$ GHz) and φ_i = tain a density plateau of $\approx 7\lambda_{40\ \mathrm{GHz}} = 5.25$ cm. The chain starts moving ntil $t = 2500 \times T_{40\ \mathrm{GHz}}$ while being probed with fixed frequency at f = field structure close to an instant where the destructive interference occ and a UTS. We clearly see the difference inside the waveguide. Wi an an be localized while they become completely masked when the is n f the return signal in the waveguide due to the interference clea Fig. 18). The interference cannot be directly observed wh usu small discrepancies between the electric field maps co resi n the case of the omnidirectional source.

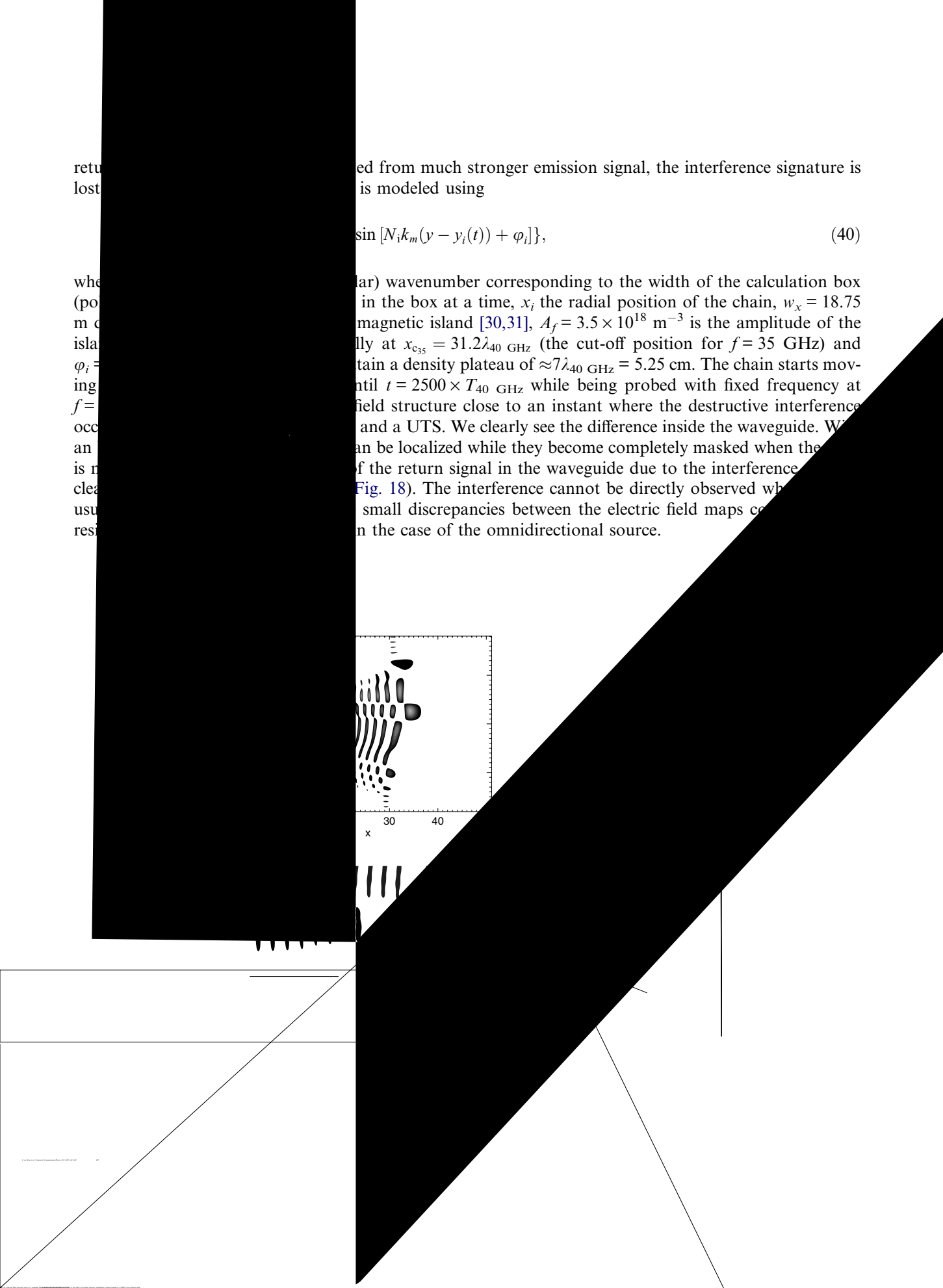

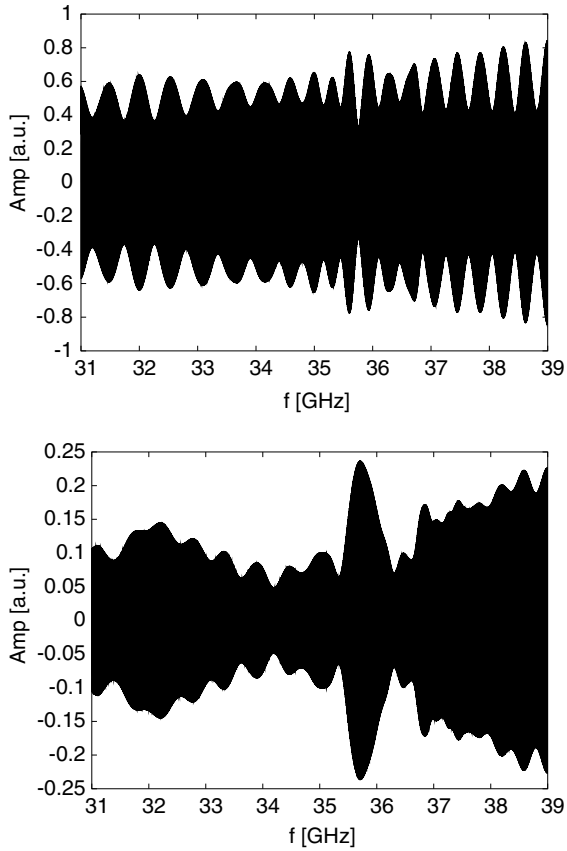

Fig. 19. Signals $E_z(i-1,j_s)$ returned by a plasma with a $q = 2$ island and turbulence probed by a CWFM wave injected without an UTS (top) and using a UTS (bottom).

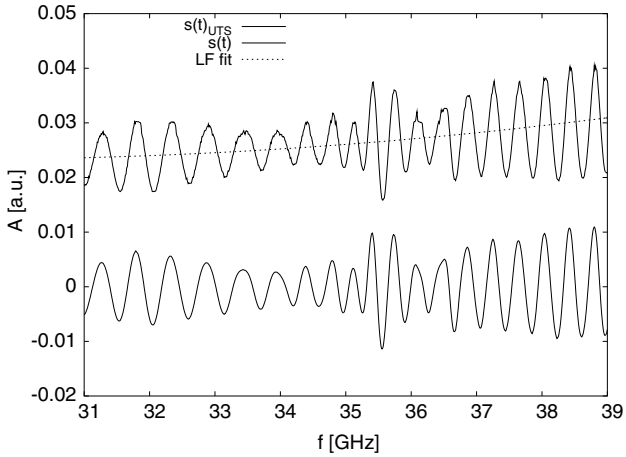

Fig. 20. Detected signals obtained with an UTS (thick line) and without (thin line).

6.3. Simulation of a $q = 2$ island with turbulence

To illustrate the advantage of using an UTS to recover the phase derivative we resort to the simulation of the effect on the reflectometry signals induced by a density perturbation due to a magnetic island present on the resonant surface $q = 2$ showing a magnitude comparable to the islands seen at ASDEX Upgrade or Tore Supra in the presence of turbulence [17]. To model it we use the expression

$$\delta n_{e_{\mathrm{mod}}} = -a(x - x_i) \exp\left[-b(x - x_i)^4\right] \mathrm{abs}\ \sin\ N_i k_m (y - y_i$$

If using a IQ detection scheme, as in this example, the results obtained using $s_{est}(t)$ (without UTS) and $s_{UTS}(t)$ differ considerably as depicted in Fig. 21 where the thick line shows the phase derivative using the UTS. This example illustrates well the need of using an UTS when using an IQ detection for the recovery of the phase derivative. Its is important to notice that even when using a SFFT without an UTS the result depends on how accurately the DC/low-frequency trend is evaluated. If the reflectometry signal has a intrinsical low frequency component this evaluation cannot be properly made and this case the use of an UTS is needed. In any case an UTS provides a cleaner signal were the chosen processing technique can be applied with less numerical operations.

7. Discussion

In this work, we have developed a numerical method for injecting a signal unidirectionally in a 2D FDTD computational grid. Although following a general formalist, the work is focused on monostatic reflectometry, where the same antenna is used as transmitter and receiver. This scheme can also be used to simulate reflectometers with different emitting and receiving antennas. In this case, the spurious reflections on the hard source line [23] are avoided. For our simulations, the type of source determines the type of reflectometer simulated: CWFM, CWFF, CWAM (Continuous Wave Amplitude Modulation), modulated Gaussian pulse and others. The technique proves itself quite useful in the simulation of CWFM reflectometry, where the frequency of the injected signal is continuously swept in frequency and the waves return to the antenna with different delays that cannot be known or predicted. This makes the use of an UTS essential to access the returned signal isolated from the emission. The use of the UTS has allowed studies on interference phenomena, due to coherent structures, and turbulence which otherwise would be extremely difficult if not impossible. The UTS method permits to choose the waveguide mode associated to the source or a linear combination of waveguide modes (in our studies we have mainly used the TE_{10} mode). The use of the impulsive response method allows the implementation of an UTS with an arbitrary time evolution of the source excitation.

The method proved to be quite fast. In fact for the size of the simulation mesh employed, the number of points used to correct the injection plays no visible role on the execution time of the code. The increase of execution time due to an augmentation of the number of points is much less than the small fluctuations on the total execution time due to other active system processes. It is important to notice that the computation time due to the UTS does not depend on the size of the box, which is not the case when Huygens surface is used [23]. Only for very small boxes (useless in practical meaningful simulations) will the time of the source correction approach the calculation time of the fields.

During the numerical tests, an interesting point observed was what happens when we remove the guiding structure (waveguide/antenna) and keep the UTS scheme. A *line* emitting transparent source is obtained. It emits in one direction as well but without the guiding structure, at the limits of the source, the fields propagates backwards. This corresponds to a source much less directive than an open waveguide and with a radiation diagram with significant side and back lobes. If a metallic plane is placed around the line the diffraction pattern of this aperture is recovered. The implementation of the UTS source on the waveguide can be an efficient way to describe a directional coupler, for example the build-up of electric field structure in a cavity powered by a unidirectional coupler can be studied. The source can also be used on a waveguide filled with a dielectric medium including its dispersion properties (i.e., a plasma). In this work we implemented the UTS to inject TE waveguide modes or a TM propagation code. The same procedure could be used to implement an UTS injecting a TM waveguide mode on an TE propagation mode. As a future work we expect to extend the impulsive response technique for the implementation of an UTS source to 3D numerical simulation.

Acknowledgment

This work, supported by the European Communities and *Instituto Superior Técnico*, has been carried out within the Contract of Association between EURATOM and IST. Financial support was also received from *Fundação para a Ciência e Tecnologia* in the frame of the Contract of Associated Laboratory. The views and opinions expressed herein do not necessarily reflect those of the European Commission, IST and FCT.

References

[1] C. Laviron, A.J.H. Donné, M.E. Manso, J. Sanchez, Reflectometry techniques for density profile measurements on fusion devices, Plasma Physics and Controlled Fusion 38 (7) (1996) 905–936.
[2] R. Sabot, J. Bottereau, J.-M. Chareau, F. Clairet, F. Gabillet, P. Hennequin, S. Heuraux, C. Honor, G. Leclert, Advances of reflectometry on Tore-Supra: from edge density profile to core density fluctuations., International Journal of Infrared and Millimeter Waves 25 (2) (2004) 229–246.
[3] K.S. Yee, Numerical solution of initial boundary value problems involving Maxwell's equations in isotropic media, IEEE Transactions on Antennas and Propagation 14 (1966) 302–307.
[4] J.B. Schneider, C.L. Wagner, O.M. Ramahi, Implementation of transparent sources in FDTD simulations, IEEE Transactions on Antennas and Propagation 46 (8) (1998) 1159–1168.
[5] A. Silva, M.E Manso, L. Cupido, M. Albrecht, F. Serra, P. Varela, J. Santos, S. Verqamota, F. Euscbio, J. Fernandas, T. Grossmann, A. Kallenbach, B. Kurzan, C. Loureiro, L. Menses, I. Nunes, F. Silva, W. Suttrrop, Ultrafast broadband frequency modulation of a continuous wave reflectometry system to measure density profiles on ASDEX Upgrade, Review of Scientific Instruments 67 (12) (1996) 4138–4145.
[6] J.G. Blaschak, G.A. Kriegsmann, A comparative study of absorbing bondary conditions, Journal of Computational Physics 77 (1988) 109–139.
[7] J.-P. Berenger, A perfectly matched layer for the absorption of electromagnetic waves, Journal of Computational Physics 114 (2) (1994) 185–200.
[8] C. Fanack, I. Boucher, S. Heuraux, G. Leclert, D. Clairet, X. Zou, Ordinary mode reflectometry: modifications of the backscattering and cut-off responses due to shape of localized density fluctuations, Plasma Physics and Controlled Fusion 38 (11) (1996) 1915–1930.
[9] J.H. Irby, S. Horne, I.H. Hutchinson, P.C. Stek, 2D full-wave simulation of ordinary mode reflectometry, Plasma Physics and Controlled Fusion 35 (5) (1993) 601–618.
[10] Y. Kogi, Measurement of cross-polarization scattering using ultrashort pulse microwaves, Review of Scientific Instruments 72 (1) (2001) 355–358.
[11] B.I. Cohen, B.B. Afeyan, A.E. Chou, N.C. Luhmann Jr., Computational study of ultra-short-pulse reflectometry, Plasma Physics and Controlled Fusion 37 (3) (1995) 329–344.
[12] B.I. Cohen, T.B. Kaiser, J.C. Garrison, One- and two-dimensional simulations of ultra-short-pulse reflectometry, Review of Scientific Instruments 68 (2) (1997) 1238–1243.
[13] B.I. Cohen, L.L. LoDestro, E.B. Hooper, T.A. Casper, Simulations of broadband short-pulse reflectometry for diagnosing plasma density and magnetic-field profiles, Plasma Physics and Controlled Fusion 40 (1) (1998) 75–89.
[14] C. Fanack, I. Boucher, F. Clairet, G. Leclert, X.L. Zou, Two-dimensional effects of radial and poloidal fluctations in ordinary mode reflectometry22nd EPS Conference on Controlled Fusion and Plasma Physics, vol. 19C, European Physical Society, 1995, p. 1152.
[15] E.Z. Gusakov, G. Leclert, I. Boucher, S. Heuraux, S. Hacquin, M. Colin, V.V. Bulanin, A.V. Petrov, B.O. Yakovlev, F. Clairet, Small-angle scattering and spatial resolution of fluctuation reflectometry: comparison of 2d analytical theory with numerical calculations, Plasma Physics and Controlled Fusion 44 (5) (2002) 1565–1579.
[16] F.d. Silva, M. Manso, A. Silva, A. Ugrade Team, Simultation of reflectometry density changes using a 2D full-wave code, Review of Scientific Instruments 72 (1) (2001) 311–314.
[17] F.d. Silva, S. Heuraux, S. Hacquin, M. Manso, Simulation of amplitude and phase variations induced by turbulence and magnetic islands on reflectometric signals, Review of Scientific Instruments 74 (3) (2003) 1497–1500.
[18] E. Holzhauer, M. Hirsch, T. Grossmann, B. Brañas, F. Serra, Theoretical and experimental investigation of the phase-runaway in microwave reflectometry, Plasma Physics and Controlled Fusion 40 (11) (1998) 1869–1886.
[19] Y. Lin, R. Nazikian, J.H. Irby, E.S. Marmar, Plasma curvature effects on microwave reflectometry fluctuation measurements, Plasma Physics and Controlled Fusion 43 (1) (2001) L1–L8.

[20] Y. Lin, J.H. Irby, R. Nazikian, E.S. Marmar, A. Mazurenko, Two-dimensional full-wave simulation of microwave reflectometry on alcator c-mod, Review of Scientific Instruments 72 (1) (2001) 344–348.
[21] E.J. Valeo, G.J. Kramer, R. Nazikian, Two-dimensional simulations of correlation reflectometry in fusion plasmas, Plasma Physics and Controlled Fusion 44 (2) (2002) L1–L11.
[22] R. Holland, J.W. Williams, Total-field versus scattered-field finite-difference codes: A comparative assessment, IEEE Transactions on Nuclear Science NS-30 (6) (1983) 4583–4588.
[23] A. Taflove, S.C. Hagness, Computational Electrodynamics: The Finite-Difference Time-Domain Method, second ed., Artech House Antennas and Propagation Library, Artech House, 2000.
[24] S. Hacquin, S. Heuraux, M. Colin, G. Leclert, Fast computations of wave propagation in an inhomogeneous plasma by a pulse compression method, Journal of Computational Physics 174 (1) (2001) 1–11.
[25] R.L. Higdon, Absorbing boundary conditions for difference approximations to the multi-dimensional wave equation, Mathematics of Computation 47 (176) (1986) 437–459.
[26] V.A. Oppenheim, R.W. Shafer, Discrete-Time Signal Processing, Signal Processing Series, Prentice Hall, NJ, 1989.
[27] S.W. Smith, The Scientist and Engineers's Guide to Digital Signal Processing, second ed., California Technical Publishing, 1999.
[28] A.B. Carlson, Communication Systems, third ed., Electrical & Electronic Engineering Series, McGraw-Hill, New York, 1987.
[29] D.M. Pozar, Microwave Engineering, first ed., Series in Electrical and Computer Enginnering, Addison-Wesley, 1993.
[30] J. Wesson, Tokamaks, third ed., International Series of Monographs on Physics, Clarendon Press, 2004, pp. 354–356 (Chapter 7).
[31] L. Vermare, F. Clairet, F. Gabrillet, R. Sabot, A. Sirinelli, S. Heuraux, G. Leclert, X-mode reflectometry for magnetohydrodynamics activity associated with $q = 1$ surface measurements on Tore Supra, Review of Scientific and Instruments 75 (10) (2004) 3825–3827.
[32] S. Heuraux, S. Hacquin, F.d. Silva, F. Clairet, R.R. Sabot, G. Leclert, Radial wave-number spectrum of density fluctuations deduced from reflectometry phase signals, Review of Scientific Instruments 74 (3) (2003) 1501–1505.
[33] P. Devynck, X. Garbet, C. Laviron, J. Payan, S.K. Saha, F. Gervais, P. Hennequin, A. Quemeneur, A. Truc, Localized measurements of turbulence in the TORE SUPRA tokamak, Plasma Physics and Controlled Fusion 35 (1) (1993) 63–76.